

# Thermal dose optimization method for ultrasound surgery

Matti Malinen, Tomi Huttunen and Jari P. Kaipio †

Department of Applied Physics, University of Kuopio, P.O. box 1627, 70211 Kuopio, Finland

**Abstract.** In this paper a model based optimization method is derived to control the thermal dose in biological tissues for ultrasound surgery. The optimization method uses the bioheat equation as a system model and quadratic cost criteria for the desired thermal dose. Time-harmonic quasi-stationary ultrasound fields are used as the heat source. In this method the optimal phase and the amplitude trajectories are found directly by minimizing the associated cost function. The approach allows also for maximum input amplitude constraints. The method is based on the Hamiltonian form of the system and results in a large dimensional nonlinear optimization problem which is solved with a gradient type iterative scheme. The performance of the optimization method is tested with 2D simulations and it is shown that the approach is able to yield a feasible nominal solution. This nominal evolution would then eventually be sought to be maintained with the help of a feedback controller during the actual sonication.

PACS numbers: 07.05.Dz, 87.50.Kk, 87.54.Br

† email: Jari.Kaipio@uku.fi

## 1. Introduction

In ultrasound surgery the cancerous tissue is destroyed by raising the thermal dose to a level that causes necrosis (Duck *et al* 1998, Daum and Hynynen 1998, Wan *et al* 1996). The control problem in ultrasound surgery is to achieve the optimal thermal dose distribution in the tissue. The main point is to raise the thermal dose in tumor region to cause necrosis while in the healthy region the thermal dose is kept as low as possible.

The controllers that are derived for ultrasound hyperthermia and ultrasound surgery usually control the temperature rather than the thermal dose. The approaches used for temperature control include PID (proportional-integral-derivative) type controllers (VanBaren and Ebbini 1995, Johnson *et al* 1990, Lin *et al* 1990), fuzzy logic (Chen *et al* 1999) and inverse dynamics approach (Mattingly *et al* 2000). The thermal dose is controlled by the temporal switching (Daum and Hynynen, 1998) or power adjusted focus scans (Wan *et al* 1996). These controllers use the pre-focused ultrasound fields with pre-determined scanning paths. With the associated approximations the resulting controllers are linear and the control variable is the power applied to the transducers. The performance of these controllers is limited due to the approximations that are made when the controller is derived.

In this paper we propose an optimization method for the feedforward control of the thermal dose in ultrasound surgery. The optimization framework is similar to the optimal feedforward control theory (Stengel 1994, Levine 1991). This approach is model-based optimization which is not based on feedback during the sonication. With this method the scanning paths and focus points are determined by the optimization algorithm. The optimization method proposed here is based on a feedforward temperature controller which has been discussed in (Malinen *et al* 2002).

In this method the time-harmonic solution of the inhomogeneous Helmholtz

equation is computed by the ultra weak variational formulation (UWVF) for each transducer individually. As compared to the other full-wave methods, UWVF reduces the computational dimensions of the problem significantly (Huttunen *et al* 2002). These pre-computed ultrasound fields are used as a heat source in the Pennes' bioheat equation. The bioheat equation is solved by semi-discrete scheme of the finite element method and it is used as the system equation in optimization framework. The quadratic cost function weights the desired thermal dose and the smoothness of the transducer excitations as a function of time. In this approach, the optimization is accomplished with respect to the real and the imaginary parts of the transducer excitations. The optimization method adjusts the real and imaginary part of each transducer individually to obtain the desired thermal dose in tissues. There are some practical limitations to the transducer excitations. First, the maximum input amplitude is limited. This limitation is solved by posing inequality constraints to the input amplitude. Second, the smoothness of the input trajectories is obtained by weighting the time derivative of the transducer excitations. The equations for optimization method are derived by using the Hamiltonian approach with Lagrange multipliers (Stengel 1994, Levine 1991). The optimal phase and amplitude trajectories are found by minimizing the cost function. This approach results in a large dimension nonlinear optimization problem which is solved by a gradient based algorithm.

## 2. Physical theory and computational methods

### 2.1. Helmholtz Problem and UWVF approximation

The space dependent part  $p$  of the time-harmonic pressure field  $P(x, t) = p(x)e^{-i\omega t}$  in heterogenous medium can be modeled using the inhomogeneous Helmholtz equation

$$\nabla \cdot \left( \frac{1}{\rho} \nabla p \right) + \frac{\kappa^2}{\rho} p = 0. \quad (1)$$

In dissipative medium the wave number is of the form  $\kappa = 2\pi f/c + i\alpha$  where  $f$  is the frequency of the wave field,  $c$  is the speed of sound and  $\alpha$  is the absorption coefficient (Bhatia, 1967). The density is denoted by  $\rho$ .

The problem at hand is to solve the pressure field radiated by the phased array consisting of  $m$  separate elements, see Fig.1. Let us denote the surface of the  $k^{\text{th}}$  element of the array by  $\Gamma_k$ . When the  $k^{\text{th}}$  element of the array is oscillating with the uniform normal velocity amplitude  $v_n$ , while the rest of the elements are passive, the field is obtained as the solution of the problem

$$\nabla \cdot \left( \frac{1}{\rho} \nabla p_k \right) + \frac{\kappa^2}{\rho} p_k = 0 \quad \text{in } \Omega \quad (2)$$

$$\frac{\partial p_k}{\partial \nu} = i2\pi f \rho v_n \quad \text{on } \Gamma_k \quad (3)$$

$$\frac{\partial p_k}{\partial \nu} = 0 \quad \text{on } \Gamma_j, \quad j \neq k \quad (4)$$

$$\frac{\partial p_k}{\partial \nu} - i\kappa p_k = 0 \quad \text{on } \Gamma_{\text{abs}}, \quad (5)$$

where  $\nu$  is outward unit normal of the boundary. The boundary condition for the passive elements (4) corresponds to the perfectly rigid surface. The computation domain  $\Omega$  is bounded by the boundary of the exterior domain  $\Gamma_{\text{abs}}$  which do not coincide with any of the elements  $\Gamma_k$ . On  $\Gamma_{\text{abs}}$  we use a zeroth order absorbing boundary condition (5).

*2.1.1. The ultra weak variational formulation.* The standard tools for solving problems like (2)-(5) have been the finite difference and finite element methods. To obtain tolerable accuracy these methods require at least ten discretization points or elements per wavelength which with high wave numbers causes intolerable computational burden. Other approaches include for example methods of ray acoustics (Botros *et al* 1997, Botros *et al* 1998), pseudospectral methods (Wojcik *et al* 1997) and k-space methods (Mast *et al* 2001).

The ultra weak variational formulation (UWVF) (Cessenat and Despres 1998) was proposed as an alternative method to reduce computational complexity related to high

frequency Helmholtz problems. The method is briefly outlined in this section. For more detailed derivation we refer to (Cessenat and Despres 1998, Huttunen *et al* 2002).

For the UWVF, we partition the computation domain  $\Omega$  with  $K$  disjoint triangular finite elements  $\Omega_j$ , Fig.2. Let  $\nu_j$  denote the outward unit normal for  $j^{\text{th}}$  element. The boundary between elements  $\Omega_j$  and  $\Omega_\ell$  is denoted by  $\Sigma_{j\ell}$ . If the element  $\Omega_j$  is on the boundary of the domain  $\Omega$ , the coinciding boundary is denoted by  $\partial\Omega_j \cap \partial\Omega = \Gamma_j$ . The parameters  $\rho$  and  $\kappa$  are approximated with piecewise constant functions. We can now decompose the Helmholtz problem (2)-(5) for all  $1 \leq j \leq K$  as

$$\Delta p_j + \kappa_j^2 p_j = 0 \quad \text{in } \Omega_j \quad (6)$$

$$\frac{1}{\rho_j} \frac{\partial p_j}{\partial \nu_j} - i\sigma p_j = -\frac{1}{\rho_\ell} \frac{\partial p_\ell}{\partial \nu_\ell} - i\sigma p_\ell \quad \text{on } \Sigma_{j\ell} \text{ and for all } \ell \quad (7)$$

$$\left( \frac{1}{\rho_j} \frac{\partial p_j}{\partial \nu_j} - i\sigma p_j \right) = \tau \left( -\frac{1}{\rho_j} \frac{\partial p_j}{\partial \nu_j} - i\sigma p_j \right) + g \quad \text{on } \Gamma_j \quad (8)$$

where  $p_j = p|_{\Omega_j}$ ,  $\tau \in \mathbb{C}$ ,  $|\tau| \leq 1$ , and the coupling parameter  $\sigma > 0$ ,  $\sigma \in \mathbb{R}$ . The boundary conditions for the problem can be adjusted with the parameter  $\tau$  and the source term  $g$ . The boundary conditions on the array surface (3) and (4) are obtained when  $\tau = 1$  and  $g = i4\pi f \rho v_n$  or  $g = 0$ , respectively. The absorbing boundary condition (5) is satisfied when  $\tau = 0$  and  $g = 0$ .

The coupled boundary condition (7) enforces the continuity of the pressure and the normal particle velocity across the interface  $\Sigma_{j\ell}$ . As the coupling parameter  $\sigma$  we have used the mean value of  $\text{Re}(\kappa)/c$  over the boundary (Benamou and Despres 1997)

$$\sigma = \frac{1}{2} \left( \frac{\text{Re}(\kappa_j)}{\rho_j} + \frac{\text{Re}(\kappa_\ell)}{\rho_\ell} \right) \quad \text{on } \Sigma_{j\ell}. \quad (9)$$

The next step is to define the function  $f$ ,  $f|_{\partial\Omega_j} = f_j$  on the element boundaries as follows

$$f_j = \left( \left( -\frac{1}{\rho_j} \frac{\partial}{\partial \nu_j} - i\sigma \right) p_j \right) \Big|_{\partial\Omega_j}, \quad 1 \leq j \leq K. \quad (10)$$

It can be shown (Cessenat and Despres 1998) that  $f_j$  satisfies

$$\sum_{j=1}^K \int_{\partial\Omega_j} \frac{1}{\sigma} f_j \overline{\left( -\frac{1}{\rho_j} \frac{\partial}{\partial \nu_j} - i\sigma \right) q_j} - \sum_{j=1}^K \sum_{\ell=1}^K \int_{\Sigma_{j\ell}} \frac{1}{\sigma} f_\ell \overline{\left( \frac{1}{\rho_j} \frac{\partial}{\partial \nu_j} - i\sigma \right) q_j}$$

$$+ \sum_{j=1}^K \int_{\Gamma_j} \frac{t}{\sigma} f_k \overline{\left( \frac{1}{\rho_j} \frac{\partial}{\partial \nu_j} - i\sigma \right)} q_j = \sum_{j=1}^K \int_{\Gamma_j} \frac{1}{\sigma} g \overline{\left( \frac{1}{\rho_j} \frac{\partial}{\partial \nu_j} - i\sigma \right)} q_j \quad (11)$$

for all test functions  $q_j$  which are the solutions of the adjoint Helmholtz equation

$$\Delta \bar{q}_j + \kappa_j^2 \bar{q}_j = 0 \quad \text{in } \Omega_j, \quad (12)$$

where the overbar denotes complex conjugation. The Equation (11) is called the ultra weak variational formulation of the Helmholtz problem.

*2.1.2. Discrete UWVF.* The major advantage of the UWVF is that it incorporates a priori information of the solution to the approximation subspace. Since the test function  $q_j$  must be a solution of the adjoint Helmholtz problem it is natural to use a Galerkin type approach to discretize the UWVF. This means that the function (10) is approximated in the test function subspace. The most obvious choice is to use plane wave basis with compact support

$$f_j^a = \sum_{n=1}^{N_j} f_{jn} \left( -\frac{1}{\rho_j} \frac{\partial}{\partial \nu_j} - i\sigma \right) \varphi_{jn} \quad (13)$$

where

$$\varphi_{jn} = \begin{cases} \exp(i\bar{\kappa}_j d_{jn} \cdot r) & \text{in } \Omega_j \\ 0 & \text{elsewhere.} \end{cases} \quad (14)$$

For simplicity, a set of equally distributed plane waves  $d_{jn}$  is usually chosen

$$d_{jn} = \left( \cos \left( 2\pi \frac{n-1}{N_j} \right), \sin \left( 2\pi \frac{n-1}{N_j} \right) \right), \quad \text{for all } j \text{ and } n.$$

Note that the functions  $\varphi_{jn}$  are also solutions of the adjoint Helmholtz problem and the Galerkin scheme is obtained by choosing  $q_j \leftarrow \varphi_{jn}$ ,  $n = 1, \dots, N_j$ .

By substituting (13) and (14) into the ultra weak variational form (11) the problem can be written in the form of the matrix equation (Cessenat and Despres 1998)

$$(I - D^{-1}C)X = D^{-1}b. \quad (15)$$

where the unknowns  $X = (f_{11}, \dots, f_{1N_1}, \dots, f_{KN_K})^T$  are to be determined. Due to the compactly supported basis functions matrices  $D$  and  $C$  are sparse and exhibit sparse

block structure. For example,  $D$  is a Hermitian block diagonal matrix consisting of the  $K$  blocks  $D_j \in \mathbb{C}^{N_j \times N_j}$ . The number of basis functions in each element can be chosen using the knowledge of the condition number of the corresponding matrix block  $D_j$  (Huttunen *et al* 2002).

From the equations (10) and (13) it follows that we can approximate the pressure field with

$$p^a = \sum_{n=1}^{N_j} f_{jn} q_{jn} \quad \text{on } \partial\Omega_j. \quad (16)$$

Although this representation for  $p^a$  is exact only on the skeleton of the mesh  $\partial\Omega_j$ ,  $j = 1, \dots, K$  it is approximately valid also within the elements.

## 2.2. The bioheat equation and the thermal dose

In biological tissue the temperature evolution is usually approximated with the bioheat equation (Pennes 1948)

$$\rho C_T \frac{\partial T}{\partial t} = \nabla \cdot k \nabla T - w_B C_B (T - T_A) + Q, \quad (17)$$

where  $T$  is temperature,  $C_T$  is the heat capacity of tissue,  $w_B$  is the perfusion due to blood flow,  $C_B$  is the heat capacity of the blood,  $T_A$  is the arterial blood temperature and  $Q$  is the heat source term. The heat source term for the time-harmonic acoustic pressure can be written as (Pierce 1991)

$$Q = \frac{\alpha |p|^2}{\rho c}. \quad (18)$$

With  $m$  transducers, the total field  $p$  can be expressed with the terms of the sum over the individual pressure fields  $p_k$

$$p = \sum_{k=1}^m p_k = \sum_{k=1}^m v_k(t) C_k(r) e^{-i\omega t}, \quad (19)$$

where  $v_k \in \mathbb{C}$  is the variable that determines the phase and amplitude of the transducer and  $C_k$  is the time-harmonic solution of the inhomogeneous Helmholtz equation with

unit amplitude incoming wave. The heat source term in Eq. (18) can be written with Eq. (19) as

$$Q(r, t) = \frac{\alpha(r)}{\rho(r)c(r)} |p|^2 = \frac{\alpha(r)}{\rho(r)c(r)} \left| \sum_{k=1}^m v_k(t) C_k(r) \right|^2. \quad (20)$$

In this study the bioheat equation is discretized by using the semi-discrete scheme. The spatial variable is approximated with Galerkin scheme and the temporal integration is accomplished by the Implicit Euler method (Johnson 1987). This standard approach can be used with the bioheat equation while the only exception is the heat source term, see (Malinen *et al* 2002).

In FE approximation of the heat source term, the parameters  $\alpha(r)$ ,  $\rho(r)$  and  $c(r)$  are approximated to be constant in each element. This approximation is valid since we are considering meshes that are conformal with the organ boundaries. In this study we also approximated  $\alpha(r)$ ,  $\rho(r)$  and  $c(r)$  to be constant in time. There are reports that have shown the temperature and the thermal dose dependence of these parameters (Gertner *et al* 1997), (Damianou *et al* 1997). However, we used commonly made approximation to keep these parameters as constant in time and neglected the effect of the temperature rise to these parameters. We approximate the intensity  $|p|^2$  in the same basis as the temperature. With these approximations the discretized heat source term  $Q_{D,j}$  in the  $j^{\text{th}}$  node can be written as

$$Q_{D,j}(t) = \sum_{p=1}^N \left| \sum_{k=1}^m \tilde{u}_k(t) \tilde{C}_k(r_p) \right|^2 \int_{\Omega} \frac{\alpha(r)}{\rho(r)c(r)} \varphi_p(r) \varphi_j(r) dr, \quad (21)$$

where  $\varphi_p$  and  $\varphi_j$  are the basis functions. The modified mass matrix  $\tilde{M} \in \mathbb{R}^{N \times N}$  for the heat source term is

$$\tilde{M}_{j,p} = \int_{\Omega} \frac{\alpha(r)}{\rho(r)c(r)} \varphi_p(r) \varphi_j(r) dr. \quad (22)$$

We define the feedforward control variables  $u_k = \text{Re } v_k$  and  $u_{k+m} = \text{Im } v_k$ ,  $k = 1, \dots, m$  and the resulting feedforward control variable  $u \in \mathbb{R}^{2m}$ . The unit amplitude waves for

each transducer are arranged as  $\widehat{C}_k = (C_k(r_1), \dots, C_k(r_N))^T$  and  $\widehat{C} = (\widehat{C}_1, \dots, \widehat{C}_m) \in \mathbb{R}^{N \times m}$ . With these changes the heat source term can be written in the form

$$Q_D(t) = \widetilde{M}[I, I] \left( Bu(t) \right)^2 = \widetilde{M}_D \left( Bu(t) \right)^2, \quad (23)$$

where  $I \in \mathbb{R}^{N \times N}$  is the identity matrix,  $(\cdot)^2$  denotes a vector with elementwise squares and

$$B = \begin{pmatrix} \text{Re } \widehat{C} & -\text{Im } \widehat{C} \\ \text{Im } \widehat{C} & \text{Re } \widehat{C} \end{pmatrix}. \quad (24)$$

The semi-discrete FEM approximation for the bioheat equation can then be written as

$$M\dot{T} = (G - w_b C_b I)T + w_b C_b M T_A + \widetilde{M}_D \left( Bu(t) \right)^2, \quad (25)$$

where  $\dot{T} = dT/dt$ ,  $M$  and  $G$  are the conventional inhomogeneous mass and stiffness matrices, respectively. After left multiplying with the inverse of the mass matrix Eq. (25) is of the form

$$\dot{T} = AT + P + M_D \left( Bu(t) \right)^2. \quad (26)$$

In the bioheat equation we used the Dirichlet boundary condition. In the Dirichlet condition the temperature was set to 37°C in the boundary of the computation domain.

The thermal dose in biological tissues is defined as (Sapareto and Dewey 1984),

$$D(T, t) = \int_0^{t_f} R^{(43-T(t))} dt, \quad R = \begin{cases} 0.25 & \text{for } T(t) < 43^\circ\text{C} \\ 0.50 & \text{for } T(t) \geq 43^\circ\text{C} \end{cases} \quad (27)$$

where  $t_f$  is the final time where dose is integrated. The unit of the thermal dose is equivalent minutes at 43°C. The level of the thermal dose that causes necrosis in most of the soft tissues is from 50 to 240 equivalent minutes at 43°C (Damianou and Hynynen 1994), (McDannold 2002).

### 3. Optimization method

We define the quadratic cost function for the system as

$$J(T, \dot{u}; t) = \frac{1}{2} \left\| D(T, t) - D_d \right\|_W^2 + \frac{1}{2} \int_0^{t_f} \sum_{k=1}^{2m} s_k \left( \dot{u}(t) \right)^2 dt, \quad (28)$$

where  $D(T, t)$  is the thermal dose and  $D_d$  is the desired thermal dose. The time derivative of the input is denoted by  $\dot{u}$ . The thermal dose distribution error is penalized with a  $W$ -norm and  $s_k$  are the scalars which weight the time derivative of the input. The Hamiltonian of the system equation (26) and the cost function (28) is of the form (Stengel 1994, Levine 1996)

$$H(T, u, \dot{u}; t) = \frac{1}{2} \left( \left\| D(T, t) - D_d \right\|_W^2 + \sum_{k=1}^{2m} s_k \left( \dot{u}(t) \right)^2 \right) + \lambda^T (AT(t) - P - M(Bu(t))^2) + \mu^T c(u(t)), \quad (29)$$

where  $\lambda(t) \in \mathbb{R}^N$  and  $\mu(t) \in \mathbb{R}^m$  are the Lagrange multipliers for the system equation and the inequality constraint respectively. The inequality constraint  $c(u(t)) \in \mathbb{R}^m$  limits the maximum applied amplitude from the ultrasound transducers. The  $i^{\text{th}}$  component of the inequality constraint is

$$c_i(u(t)) = \begin{cases} K \left( (u_i^2(t) + u_{m+i}^2(t))^{1/2} - u_{\max,k} \right)^2, & \text{if } (u_i^2(t) + u_{m+i}^2(t))^{1/2} \geq u_{\max,k} \\ 0, & \text{if } (u_i^2(t) + u_{m+i}^2(t))^{1/2} < u_{\max,k} \end{cases} \quad (30)$$

where  $K$  is the weighting scalar,  $u_{\max,k}$  is the maximum amplitude during the  $k^{\text{th}}$  time interval in sonication and  $i = 1, \dots, m$ .

The equations for optimization method are derived via the temporal discretization of the Hamiltonian form in Eq. (29). Let the time step for temporal discretization be  $\Delta t$ . We discretize the time interval  $t = 0, \dots, t_f$ , thus  $N_t = t_f/\Delta t + 1$ . In the following the temporally discretized variables are denoted by subscript  $t$ , so that we have  $u_t = u(t\tau/\Delta t)$ ,  $\tau \in [0, t_f]$ ,  $t \in [0, \dots, N_t]$ . The temporally discretized Hamiltonian is of the form

$$H(T_t, u_t) = \frac{1}{2} \left( (D - D_d)^T W (D - D_d) + (u_t - u_{t-1})^T S (u_t - u_{t-1}) \right)$$

$$+ \lambda_t (AT_t + P + M_D(Bu_t)^2) + \mu_t c(u_t), \quad (31)$$

where  $S = \text{diag}(s_1, \dots, s_{2m})$  and  $W$  is the positive definite weighting matrix. The time derivative of the Lagrange multiplier  $\lambda(t)$  for the system equation is characterized by the co-state equation (Stengel 1994). In this case we have for the co-state equation

$$\frac{\partial \lambda}{\partial t} = \frac{\partial H}{\partial T_t} = W(D - D_d) \odot \ln(R)R^{(43-T_t)} + A^T \lambda_t, \quad (32)$$

where  $\odot$  denotes the elementwise product. The stationary condition that characterizes the local minimum can be written as

$$H_{u_t} = \frac{\partial H}{\partial u_t} = S(u_t - u_{t-1}) + F(u_t)^T \lambda_t + c_{u_t}(u_t)^T \mu_t = 0 \quad (33)$$

$$F(u_t) = 2M_D \left( B \odot (Bu_t, \dots, Bu_t) \right) \in \mathbb{R}^{N \times 2m}$$

$$c_{u_t}(u_t) = \frac{\partial c(u_t)}{\partial u_t} = D \in \mathbb{R}^{m \times 2m}, \quad \text{where}$$

$$D_{i,i} = 2K u_{i,t} \frac{((u_{i,t}^2 + u_{m+i,t}^2)^{1/2} - u_{\max_k})}{(u_{i,t}^2 + u_{m+i,t}^2)^{1/2}}, \quad i = 1, \dots, m$$

$$D_{i,m+i} = 2K u_{m+i,t} \frac{((u_{i,t}^2 + u_{m+i,t}^2)^{1/2} - u_{\max_k})}{(u_{i,t}^2 + u_{m+i,t}^2)^{1/2}}, \quad i = 1, \dots, m$$

where  $j = 1, \dots, 2m$  and  $\Delta t^{-2}$  is absorbed into matrix  $S$ . The Lagrange multiplier for the inequality constraint can be solved from Eq. (33). After rearranging terms we obtain

$$\mu_t = - (c_{u_t}(u_t)^T)^\dagger (F(u_t)^T \lambda_t + S(u_t - u_{t-1})), \quad (34)$$

where  $\dagger$  denotes the pseudoinverse. The stationary condition can be solved by substituting Eq. (34) into Eq. (33).

The time evolution for the bioheat equation and the co-state equation is computed by the implicit Euler iteration. The implicit Euler forms of the equations (26) and (32) are

$$T_{t+1} = (I - \Delta t A)^{-1} T_t + \Delta t (I - \Delta t A)^{-1} (P - M_D (Bu_t)^2) \quad (35)$$

$$\lambda_{t-1} = (I - \Delta t A^T)^{-1} \lambda_t + \Delta t (I - \Delta t A^T)^{-1} (W(D - D_d) \odot \ln(R)R^{43-T_t}) \quad (36)$$

The stationary condition is solved by using a Levenberg-Marquardt type stabilized search

$$H_{u_t} = \left( F(u_t)^T F(u_t) + \gamma I \right)^{-1} \left( S(u_t - u_{t-1}) + c_{u_t}(u_t)^T \mu_t + F(u_t)^T \lambda_t \right) \quad (37)$$

where  $\gamma$  is the stabilization parameter. In the optimization algorithm iteration inputs are computed as

$$u_t^{(\ell+1)} = u_t^{(\ell)} + \epsilon^{(\ell)} H_{u_t}^{(\ell)} \quad (38)$$

where  $\ell$  is the iteration number and  $\epsilon^{(\ell)}$  is the corresponding iteration step parameter. In thermal dose optimization the magnitude of the gradient  $H_{u_t}^{(\ell)}$  varies significantly during the iteration. The iteration step parameter at iteration  $\ell$  is chosen so that the pointwise correction to the new input value  $u_t^{(\ell+1)}$  from  $H_{u_t}^{(\ell)}$  is less than 0.1.

The optimization algorithm iteration consists of the following six steps: 1. The system equation is solved from Eq. (35). 2. The Lagrange multiplier for the system equation is solved from Eq. (21). 3. The Lagrange multiplier for inequality constraint is solved from Eq. (34). 5. The stationary condition is solved from Eq. (37). 6. The new value of the input is computed from Eq. (38). This procedure is repeated until relative error in the values of the cost function in Eq. (28) between two successive iterations is below a predetermined value.

## 4. Simulations

### 4.1. Pressure field computation

The simulations were accomplished in 2D domain which is shown in Fig. 1. The domain is adopted from the sagittal CT image including the part of the liver. The domain consists of the eight subdomains which are denoted by  $\Omega_I, \dots, \Omega_{VIII}$ . The subdomains are chosen so that  $\Omega_I$  is the water layer between the transducer array and the skin ( $\Omega_{II}$ ). The subdomain  $\Omega_{III}$  is the fat layer and  $\Omega_{IV}$  represents the muscle with two ribs ( $\Omega_V$

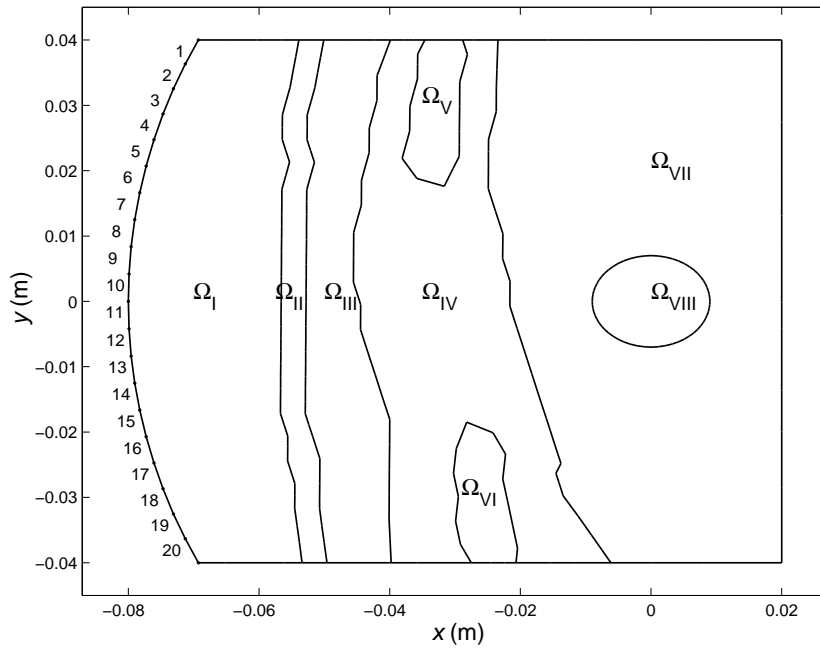


**Figure 1.** The computing domain with 20 ultrasound transducers in the left side (numbered 1, . . . , 20.) The acoustic parameters for subdomains are given in Table 1 and the thermal parameters are given in Table 2.

and  $\Omega_{VI}$ ) included. The subdomain  $\Omega_{VII}$  is the liver and  $\Omega_{VIII}$  is the cancerous tissue in the liver. The acoustic parameters for the subdomains are given in Table 1. The computing domain was divided into a mesh with 2010 elements and 1050 vertex nodes. The meshing was chosen to be conformal to the anatomical organ boundaries. In this case the mesh was finer where sharp boundaries existed between the organs.

In the simulation 20, ultrasound transducers were located in the sector of a circle with radius of 8 cm in the left side of the domain (see Fig. 1). The geometrical focus of the transducers was aimed at the middle of the cancer. The pressure field of each transducer was computed by solving the Helmholtz equation with UWVF. The frequency of the ultrasound fields were set to 500 kHz.

The accuracy of the UWVF approximation was verified by comparing the solution in the homogeneous (muscle) tissue with the numerical approximation of the Rayleigh integral. Comparison for the transducer number 10 is shown in Fig. 3. The difference of

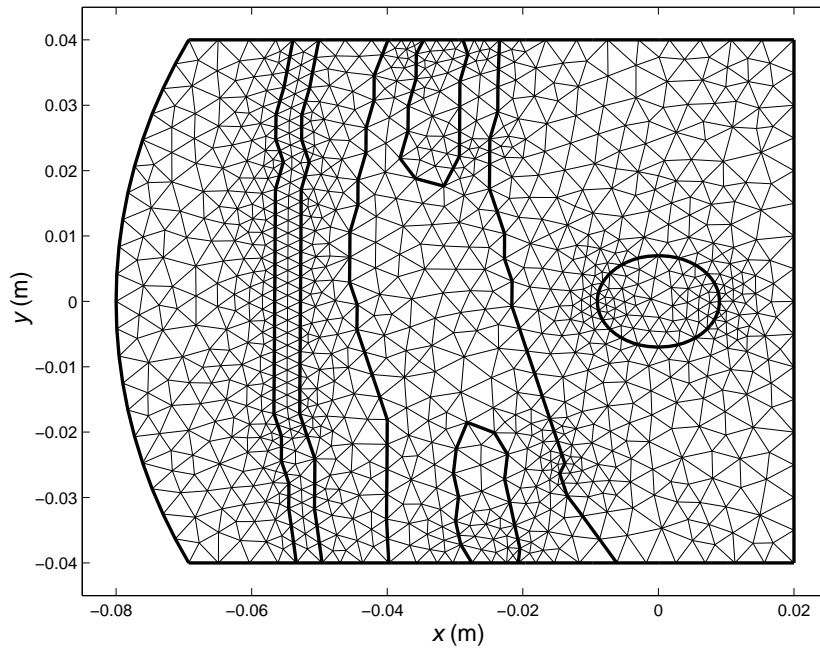


**Figure 2.** The computing mesh with 1050 nodes and 2010 elements.

**Table 1.** The acoustic parameters for simulations

Subdomain	$\alpha$ (Nep/m)	$c$ (m/s)	$\rho$ (kg/m <sup>3</sup> )
$\Omega_I$ (water)	0 <sup>a</sup>	1524 <sup>a</sup>	993 <sup>a</sup>
$\Omega_{II}$ (skin)	12 <sup>b</sup>	1610 <sup>b</sup>	1200 <sup>c</sup>
$\Omega_{III}$ (fat)	4 <sup>d</sup>	1478 <sup>a</sup>	950 <sup>a</sup>
$\Omega_{IV}$ (muscle)	5 <sup>b,c</sup>	1547 <sup>a</sup>	1050 <sup>a</sup>
$\Omega_V$ (rib)	46 <sup>b</sup>	3540 <sup>a</sup>	1990 <sup>a</sup>
$\Omega_{VI}$ (rib)	46 <sup>b</sup>	3540 <sup>a</sup>	1990 <sup>a</sup>
$\Omega_{VII}$ (liver)	2.3 <sup>b</sup>	1590 <sup>c</sup>	1060 <sup>c</sup>
$\Omega_{VIII}$ (cancer)	4 <sup>d</sup>	1590 <sup>c</sup>	1060 <sup>c</sup>

<sup>a</sup> (Mast *et al* 1999)

<sup>b</sup> (Duck 1998)

<sup>c</sup> (Gautherie 1990)

<sup>d</sup> (Goss *et al* 1980)

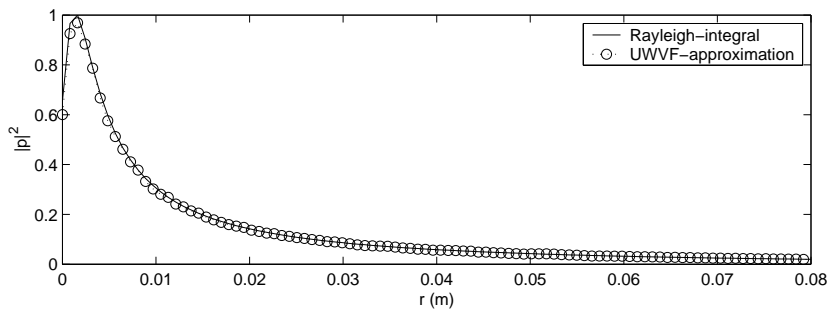


**Figure 3.** The comparison of UWVF-approximation and solution of the Rayleigh integral along the central axis of the transducer 10 in the homogeneous medium. The other transducers were not active.

the solutions in the central axis was 2% and in the whole domain 7%. The difference of the approximations did not decrease with the increase of the number of basis functions. This indicates that the difference was due to the modeling error related to the zeroth order absorbing boundary condition (5). However, there are no limitations in UWVF to use the higher order absorbing boundary condition to obtain the better accuracy. Figure 3 indicates that the meshing near the transducer element is dense enough. The transducers used in this study are relatively small and they oscillate with constant amplitude. In this case there are no sharp pressure gradients in the near field.

The number of basis functions was chosen by limiting the condition number of the matrix blocks  $D_j$  below  $10^8$ , see (Huttunen *et al* 2002). This resulted in 12-25 basis functions per element in the homogeneous test problem and 7-25 basis functions per element in the inhomogeneous problems in the mesh shown in Fig 2. The solution of the inhomogeneous problem for the element 10 is shown in Fig. 4.

Due to strong acoustical mismatch between the ribs and soft tissues, shadow regions are seen behind the ribs. The fields in the ribs were also modeled with the Helmholtz equation which ignores the possible generation of shear waves in bone. However, this a commonly made simplification , see e.g. (Mast *et al* 1999).

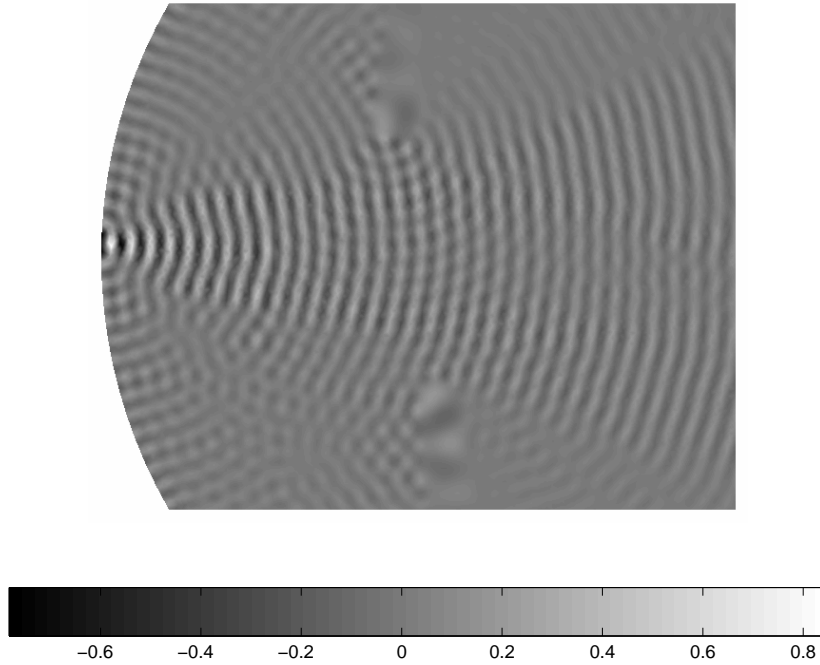


**Figure 4.** The normed UWVf-approximation of the field for the transducer 10.

#### 4.2. The thermal dose optimization

The thermal parameters of the subdomains are given in Table 2. The heat capacity of the blood was set to 3770 J/KgK in the simulation. The bioheat equation was computed by the semi-discrete FEM with implicit Euler iteration. The time interval  $t = [0, 240]$  s was discretized with  $\Delta t = 0.15$  s. The computation of the bioheat equation was accomplished in the same mesh as the Helmholtz equation.

The optimization problem was to obtain the thermal dose of 300 equivalent minutes in the cancer region while keeping the dose in other subdomains as low as possible. So the target dose distribution  $D_d$  was set to 300 equivalent minutes in cancer region and in other subdomains to zero. The desired thermal dose was chosen to be somewhat larger than the level that causes the necrosis in tissue (240 equivalent minutes at 43°C). With this high desired thermal dose we attempt to ensure the necrosis of the cancerous tissue.

**Table 2.** The thermal parameters for simulations

Subdomain	$k$ (W/mK)	$C_T$ (J/kgK)	$w_B$ (kg/m <sup>3</sup> s)
$\Omega_I$ (water)	0.63 <sup>a</sup>	4178 <sup>a</sup>	0 <sup>a</sup>
$\Omega_{II}$ (skin)	0.50 <sup>a</sup>	3770 <sup>a</sup>	1 <sup>a</sup>
$\Omega_{III}$ (fat)	0.21 <sup>b</sup>	3500 <sup>b</sup>	0.5 <sup>b</sup>
$\Omega_{IV}$ (muscle)	0.64 <sup>b</sup>	3500 <sup>b</sup>	2.3 <sup>b</sup>
$\Omega_V$ (rib)	0.44 <sup>b</sup>	1000 <sup>b</sup>	0.5 <sup>b</sup>
$\Omega_{VI}$ (rib)	0.44 <sup>b</sup>	1000 <sup>b</sup>	0.5 <sup>b</sup>
$\Omega_{VII}$ (liver)	0.64 <sup>b</sup>	3500 <sup>b</sup>	16 <sup>b</sup>
$\Omega_{VIII}$ (cancer)	0.57 <sup>c</sup>	3960 <sup>c</sup>	4 <sup>c</sup>

<sup>a</sup> (Mahoney *et al* 2001)

<sup>b</sup> (Lang *et al* 1999)

<sup>c</sup> (Liang *et al* 2001)

These criteria result in an intrinsically difficult optimization problem, since there are highly absorbing layers between the target and the transducers. The absorption and the scattering in the skin ( $\Omega_{II}$ ), muscle ( $\Omega_{IV}$ ) and ribs ( $\Omega_V$  and  $\Omega_{VI}$ ) is high and we desire to keep the thermal dose in these regions as low as possible. The other problem in the dose optimization is the large extent of the cancer.

The second design criteria concerned the control input. To test the inequality constraint, the maximum amplitude was set to  $u_{\max,1} = 0.9$  MPa for  $t \in [0, 45]$  s and  $u_{\max,2} = 0.02$  MPa for  $t \in [45, 240]$  s. Thus the constraint  $u_{\max,1}$  corresponds to the sonication time (i.e. when the transducers are on) and  $u_{\max,2}$  sets the transducers effectively off after sonication. The maximum amplitude of the transducers depends on the sonication system. Of course, the use of the Helmholtz model in this paper is tantamount to assuming that nonlinear effects do not take place. The  $u_{\max,2}$  cannot be set to zero for numerical reasons. During the iteration, the Lagrange multiplier for the system equation is computed backwards in time. If the input is set to zero in the

later part, the optimization algorithm will fail to find the local minimum. However, the constraint  $u_{\max,2} = 0.02$  MPa results in a very small absorption, which means that transducers are effectively off during the later part of the sonication. The transient time after transducers are turned off has to be taken into account in the optimization, since a significant share of the thermal dose is accumulated during the time when the tissue cools back to the ambient temperature. The smoothing of the control variable trajectories as a function of time was done by setting the weighting scalar  $K = 5000$  for the time derivative of the input.

The weights were adjusted so that the healthy region does not get too much thermal dose. The thermal dose in the healthy region was aimed to be less than 60 equivalent minutes to prevent the necrosis of the tissue. Several simulations were accomplished to find out a feasible range of weights for different tissues. The simulations resulted in the following weighting. The weighting matrix  $W$  for the thermal dose distribution was set to a diagonal matrix. The weight of 1200 was chosen for the nodes in  $\Omega_{\text{II}}, \dots, \Omega_{\text{VI}}$ . These regions are most likely to suffer from undesired thermal dose in this case. The nodes in subdomains ( $\Omega_{\text{I}}$ ) and  $\Omega_{\text{VII}}$  were weighted by zero. In simulation we assumed rather high perfusion in the liver. The simulations showed that with this high perfusion the thermal dose in liver does not reach a dangerous levels without weighting. However, if the perfusion in liver is smaller, the weighting in liver region can be increased to prevent the undesired necrosis. In the cancer domain ( $\Omega_{\text{VIII}}$ ) the nodes were weighted with 2000 to obtain the desired thermal dose.

The Levenberg-Marquardt parameter was chosen to  $\gamma = 5000$ , which corresponds to the standard choice  $\gamma = 0.05 \|F(u_t^{(0)})^T F(u_t^{(0)})\|$ . The iteration step parameter varied from  $\epsilon^{(\ell)} = 0.1, \dots, 10^{-9}$  during the iteration. The step parameter was adjusted according to the maximum value of the  $H_{u_t}^{(\ell)}$ . The reason for the wide range of  $\epsilon^{(\ell)}$  is that at the beginning of the iteration the value of the  $H_{u_t}^{(\ell)}$  is of the order  $10^{-4}$  but

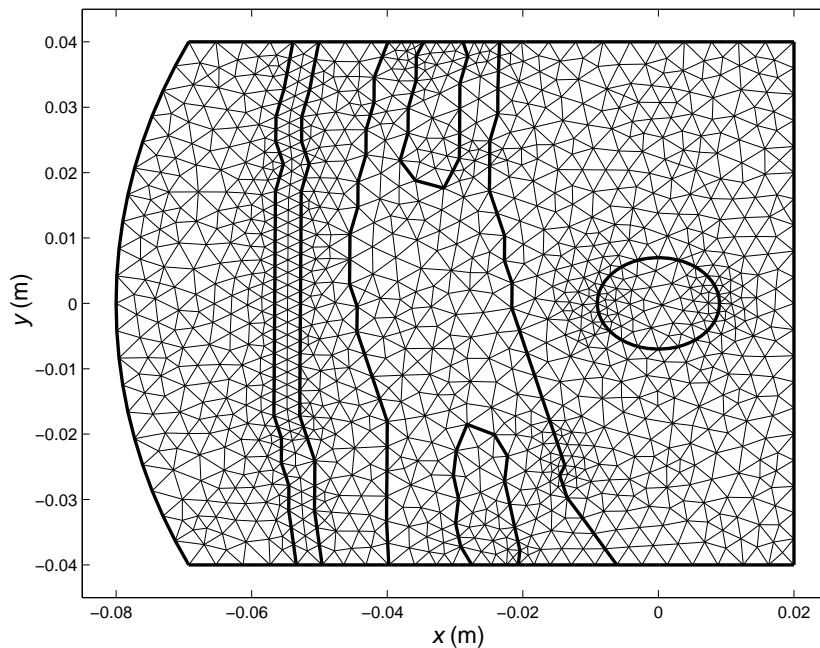


**Figure 5.** The mesh where results was verified. This mesh consists of 1203 nodes and 2309 elements.

later when the thermal dose distribution is formed the value of  $H_{u_t}^{(\ell)}$  is of the order  $10^4$ . The non-uniqueness of the phase was solved by setting the phase of the first (number 1) transducer to zero. The initial guess for the iteration was  $u_{i,t}^{(0)} = 0.01$  for all  $i$  and  $t$ . The stopping criterion for the iteration was

$$\frac{J^{(\ell)} - J^{(\ell-1)}}{J^{(\ell)}} \leq 10^{-5}, \quad (39)$$

where  $J^{(\ell)}$  is the cost at iteration  $\ell$ . Using these parameters, the algorithm took 2109 iterations to satisfy the stopping criterion. Several simulations were accomplished with different weightings for the thermal dose distribution. The algorithm took typically 500-2500 iterations to satisfy the stopping criterion in simulations.

The verification of the results in the same mesh in which the optimization is computed is sometimes called “the inverse crime”. To avoid this inverse crime we verify the results in the mesh that is shown in Fig. 5. This mesh consists of 2309 elements and 1203 nodes. The cross-checking did not have a significant effect to the results which

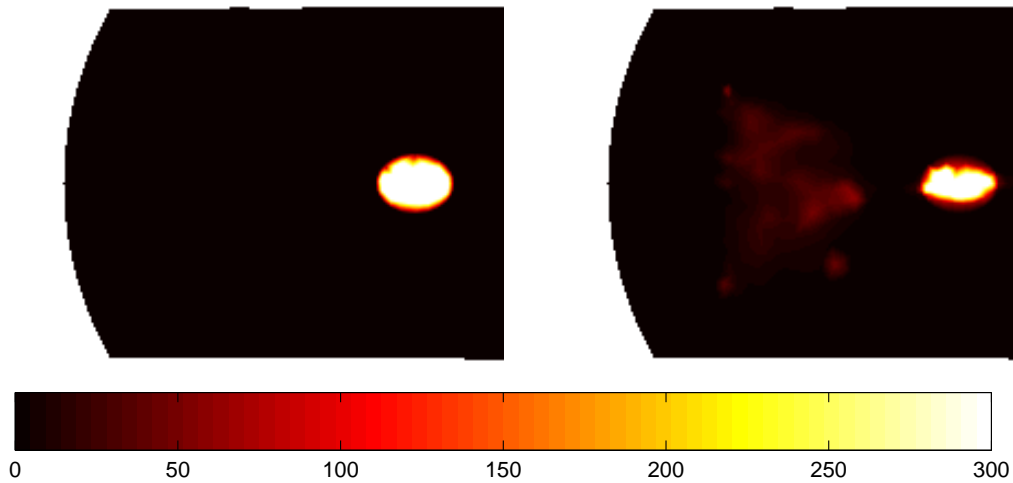


**Figure 6.** The target thermal dose distribution (left) and the controlled thermal dose distribution at the final time  $t_f=240$  s (right). The desired thermal dose in target was 300 equivalent minutes at  $43^\circ\text{C}$ .

indicates that the computing mesh was dense enough.

The target and the optimized thermal dose distribution at the final time  $t_f = 240$  s are shown in Fig. 6. The thermal dose of 240 equivalent minutes or greater is achieved in 56 % of the cancer area. Fig. 6 shows that the thermal dose in healthy subdomains is quite low. The maximum and the average thermal doses in subdomains are given in Table 3. These results show that the thermal dose in tumor region is the order of hundreds of equivalent minutes in  $43^\circ\text{C}$  and in healthy region the thermal dose is the order of tens equivalent minutes in  $43^\circ\text{C}$  or even less. The design criteria for healthy tissue is valid in all subdomains except muscle where thermal dose is 62.7 equivalent minutes. This indicates that the healthy tissue is saved while half of the cancer area is in necrosis. Fig. 7 shows the contours of the thermal dose distribution. The greatest part of the thermal dose is in the target region and there are only small dose peaks in the skin and muscle.

In design criteria, we desired to keep the thermal dose in healthy subdomains low. The results show that this aim was successful. The whole cancer can be destroyed by

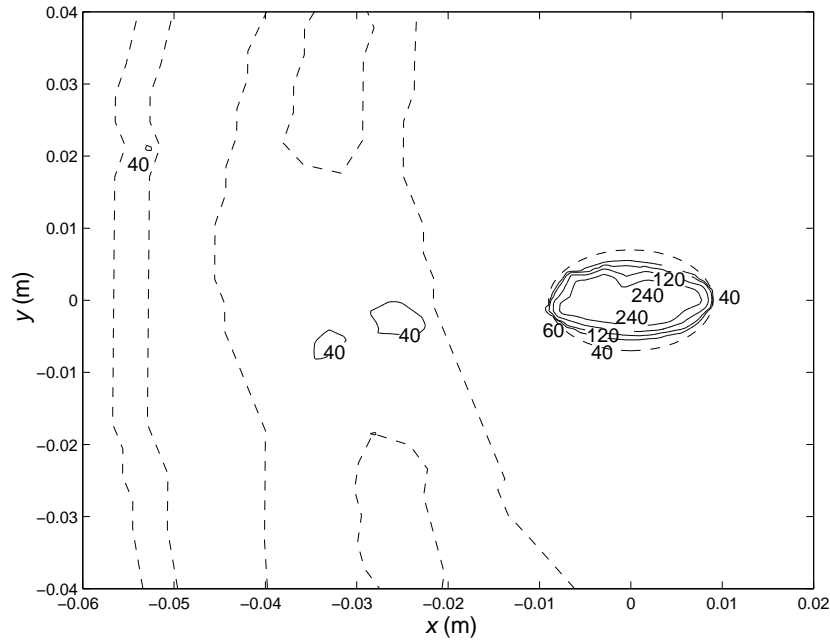
**Table 3.** The controlled maximum thermal dose ( $D_{\max}$ ) and average thermal dose ( $D_{\text{ave}}$ ) in subdomains. Units are equivalent minutes at 43°C.

Subdomain	$D_{\max}$	$D_{\text{ave}}$
$\Omega_{\text{II}}$ (skin)	53.4	3.1
$\Omega_{\text{III}}$ (fat)	31.2	7.3
$\Omega_{\text{IV}}$ (muscle)	62.7	4.7
$\Omega_{\text{V}}$ (rib)	0.3	0.05
$\Omega_{\text{VI}}$ (rib)	1.2	0.07
$\Omega_{\text{VII}}$ (liver)	59.8	1.0
$\Omega_{\text{VIII}}$ (cancer)	404.2	191.2

multiple sonications or decreasing the weight in healthy subdomains. When larger hot spots are allowed in healthy subdomains or the treatment time is longer the cancer can be completely destroyed.

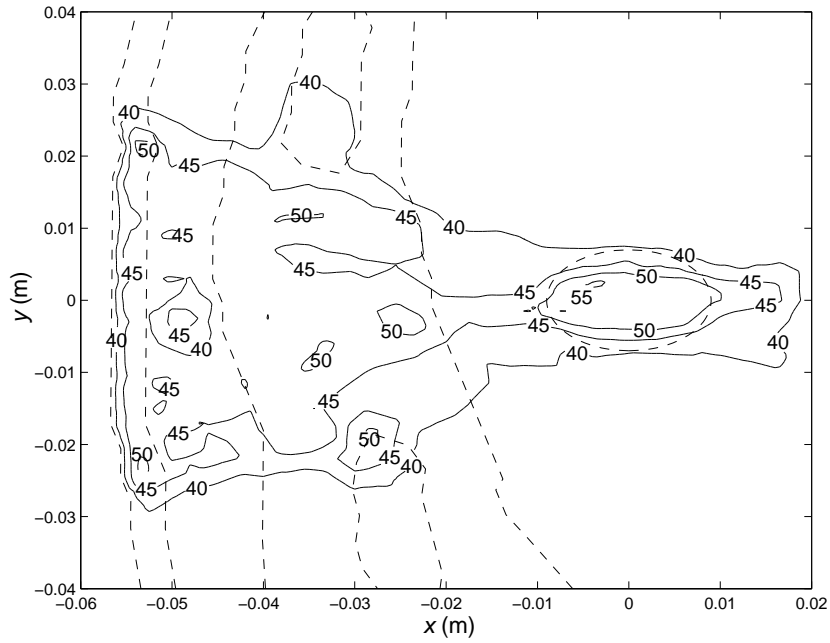
The maximum temperatures in subdomains was achieved at  $t = 45$  s which is the time when the transducers are turned off. Figure 8 shows the temperature contours at  $t = 45$  s, and this indicates that the temperatures over 50°C are only in the small parts of the healthy subdomains. This results in rapid cooling of these “hot spots” and the thermal dose does not reach dangerous level. In the major part of the healthy subdomains the temperature is reasonably low. In the simulations we took into account the cooling period of 195 s. The maximum temperature in healthy tissues was in fat 41.1°C and the maximum temperature in cancer region was 39.9°C at  $t_f = 240$  s. The cooling period is adequate and the thermal dose does not build up significantly in any subdomain after the final time.

Figure 9 shows the transducer excitations for transducers 2, 8, 10 and 18. The transducers where chosen to give the information from transducer array overall. For example, there is a rib between transducers 2 and 18 and the tumor area. Figure 9



**Figure 7.** Thermal dose contours at the final time  $t_f = 240$  s sonication. The contour lines represent the thermal doses of 40, 60, 120 and 240 equivalent minutes at  $43^\circ\text{C}$ . The anatomical structures are presented with the dashed line. The main part of the absorbed dose is in the cancer region.

shows that the amplitude from these transducers are smaller than for transducers 8 and 10. In the optimization criteria we also set limitations to the transducer excitations. First, the maximum amplitude during the early part of the sonication ( $t = 0, \dots, 45$  s) was 0.9 MPa and in later part ( $t = 45, \dots, 240$  s) 0.02 MPa. Figure 9 shows that this constraint is satisfied. The actual maximum amplitude of all the sources was 0.903 MPa and after the effective cut-off 0.0211 MPa which was due to employing penalties instead of exact inequality constraints. Second, there was a cost assigned for the time derivatives of the input trajectories. This criteria is also valid as shown Fig. 9. There are no oscillation in input trajectories. However, if the input trajectories are desired to be smoother, this can be done by increasing the weight to the time derivatives of the input.



**Figure 8.** Temperature contours at  $t = 45$  s. The contour lines are 40, 45, 50 and 55°C. Anatomical structures are presented with the dashed line. There are several hot spots in the healthy subdomains.

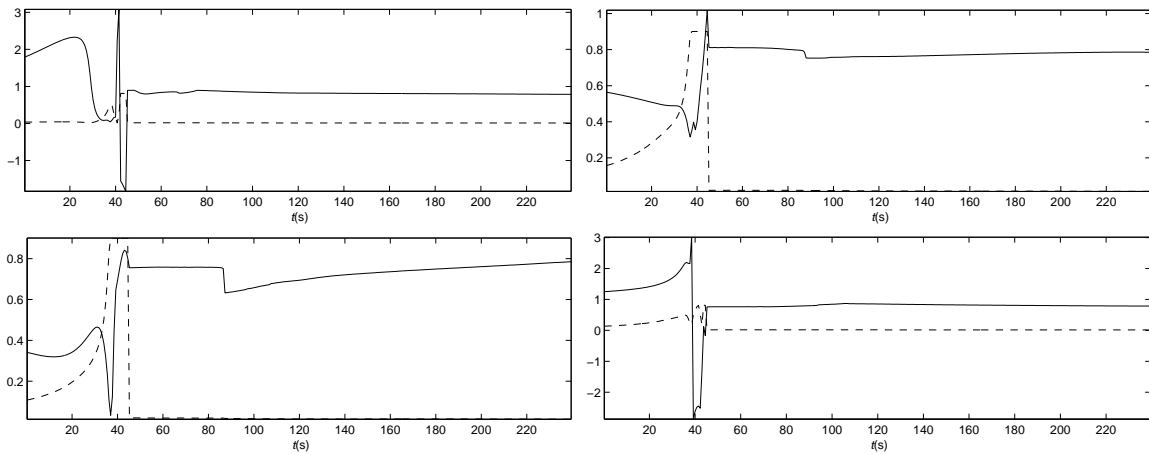


**Figure 9.** The amplitudes (dashed) and the phases (solid) for transducers 2 (top left), 10 (top right) 14 (lower left) and 18 (lower right).

## 5. Conclusions

An optimization method for the thermal dose optimization in ultrasound surgery has been proposed in this paper. The optimization method is not based on pre-focused ultrasound fields or pre-determined scanning path. The optimal thermal dose distribution is found directly by determining the phases and the amplitudes of the transducers as functions of time. The advantage of this type of optimization is that the accumulated thermal dose after the transducers are turned off can be taken into account. Also, by direct adjusting of the phases and amplitudes the thermal dose accumulation in healthy regions can be minimized. With pre-focused ultrasound fields the side lobes can cause the undesired thermal dose peaks in healthy regions.

The optimization method was tested with a 2D simulation. The result from the simulation shows that the proposed method is capable of controlling the thermal dose in strongly absorbing and scattering media in which the distribution of inhomogeneities is nontrivial. With the proposed optimization structure it is straightforward to choose the balance between the extent of destroyed cancerous and healthy tissue regions.

In the simulation we used the temperature independent acoustic and thermal parameters. Some of these parameters, for example the absorption coefficient can change during the heating (Damianou *et al* 1997, Gertner *et al* 1997). However the changes in absorption coefficient is reported to be relatively small below 55°C. In this study the maximum temperature in subdomains was 55.9°C so the approximation of the temperature independent absorption is valid. With higher temperatures, the temperature dependent absorption can be included to the optimization framework, since the solution is obtained from the iterative algorithm. The incorporation of temperature dependent coefficients is straightforward and the only effect is the slowing down of the algorithm since some matrices become state dependent.

Another approximation in the simulation was that there are no large blood vessel

included. The large blood vessels can have a significant effect to the resulting thermal dose distribution in tissues (Kolios *et al* 1996). The computational domain can be adopted from the CT or MRI image where detailed anatomical structure like large blood vessels can be identified. The perfusion in blood vessels can be then set to correspond to the volume of the vessel. As in the temperature dependent absorption case, temperature dependent perfusion can be included to the FE model in a straightforward manner.

The simulation was accomplished in 2D. In practice the control of the thermal dose has to be done in 3D. There are no intrinsic limitations to use the proposed method in the 3D control of the thermal dose. It is well known that 2D boundary control is physically and mathematically more difficult than in 3D. Only the computational issues are somewhat more difficult in 3D, in this case mainly due to the number of unknowns in the solution of the Helmholtz problem.

The proposed approach belongs to the model based optimization class. There are two sources of errors in the model. First, the crude approximations that are inherent in the Pennes bioheat model and second, the approximative distribution of density, sound speed and absorption coefficients that affect the computed pressure fields. These errors can be estimated to be so significant that any model based type approach can not be considered as a solution to the overall control approach. On the other hand, the use of a feedback controller only may not be an optimal solution either. This is due to the fact that feedback controllers can not take into account the dose that accumulated after the turn-off of the ultrasound sources. Thus it can be conjectured that a feasible overall approach is to first compute a model based optimization which is based on approximative models to yield a nominal input trajectories which takes into account the latent accumulation of thermal dose. In the second phase a feedback controller is constructed which uses MRI based temperature estimates (Kuroda *et al* 1996, McDannold *et al* 1998) and adjusts the precomputed trajectories in real time to

compensate for the suboptimal optimization. The proposed model is thus aimed to solve the first phase of the overall optimization scheme.

## Acknowledgements

The project is supported by the Finnish Academy Grants 77818, 72431 and 66592.

## References

- Benamou J D and Despres B 1997 A domain decomposition method for the Helmholtz equation and related optimal control problems *J. Comput. Phys.* **136** 68-82
- Bhatia A B 1967 *Ultrasonic absorption: an introduction to the theory of sound absorption and dispersion in gases, liquids and solids* (New York: Dover Publications, Inc.)
- Botros Y Y, Volakis J L, VanBaren P and Ebbini E S 1997 A hybrid computational model for ultrasound phased-array heating in presence of strongly scattering obstacles *IEEE Trans. Biomed. Eng.* **44** 1039-1050
- Botros Y Y, Ebbini E S and Volakis J L 1998 Two-step virtual array-ray (VAR) technique for focusing through the rib cage *IEEE Trans. Ultrason. Ferroelectr. Freq. Control* **45** 989-1000
- Cessenat O and Depres B 1998 Application of an ultra weak variational formulation of Elliptic PDEs to the two dimensional Helmholtz problem *SIAM J. Numer. Anal.* **35** 255-299
- Chen Y Y, Lin W L, Liou H L, Yen J Y and Shieh M J 1999 Self-tuning fuzzy logic control for ultrasound hyperthermia with reference temperature based on objective functions *Med. Phys.* **26** 825-833
- Damianou C A, Sanghvi N T, Fry F J and Maass-Moreno R 1997 Dependence of ultrasonic attenuation and absorption in dog soft tissues on temperature and thermal dose *J. Acoust. Soc. Am.* **102** 628-634
- Damianou C and Hynynen K 1994 The effect of various physical parameters on the size and the shape of necrosed tissue volume during ultrasound surgery *J. Acoust. Soc. Am.* **95** 1641-1649
- Daum D R and Hynynen K 1998 Thermal dose optimization via temporal switching in ultrasound surgery *IEEE Trans. Ultrason. Ferroelectr. Freq. Control* **45** 208-215
- Duck F A, Baker A C and Starrit H C 1998 *Ultrasound in medicine* (London: Institute of Physics Publishing)
- Gautherie M 1990 *Methods of External Hyperthermic Heating* (Berlin: Springer-Verlag)

- Gertner M R, Wilson B C and Sherar M D 1997 Ultrasound properties of liver tissue during heating  
*Ultrasound in Med. & Biol.* **23** 1395-1403
- Goss S A, Johnston R L and Dunn F 1980 Compilation of empirical ultrasonic properties of mammalian tissues II *J. Acoust. Soc. Am.* **68** 93-108
- Huttunen T, Monk P and Kaipio J P 2002 Computational aspects of the ultraweak variational formulation *J. Comput. Phys.* accepted for publication.
- Johnson C 1987 *Numerical solution of the partial differential equations by the finite element method* (Lund: Studentlitteratur)
- Johnson C, Kress R, Roemer B and Hynynen K 1990 Multi-point feedback control system for scanned, focused ultrasound hyperthermia *Phys. Med. Biol.* **35** 781-786
- Kolios M C, Sherar M D, Hunt J W 1996 Blood flow cooling and ultrasound lesion formation *Med. Phys.* **7** 1287-1298
- Kuroda K Y, Suzuki Y, Ishihara Y and Okamoto K 1996 Temperature mapping using water proton chemical shift obtained with 3D-MRSI: feasibility in vivo. *Magn. Reson. Med.* **35** 20-29
- Lang J, Erdmann B and Seebass M 1999 Impact of nonlinear heat transfer on temperature control in regional hyperthermia *IEEE Trans. Biomed. Eng.* **46** 1129-1138
- Levine W S 1996 *The control handbook* (Boca Raton: CRC Press, Inc.)
- Liang P, Dong B, Yu X, Yu D, Cheng Z, Su L, Peng J, Nan Q and Wang H 2001 Computer-aided simulation of microwave-induced thermal distribution in coagulation of liver cancer *IEEE Trans. Biomed. Eng.* **48** 821-829
- Lin W L, Roemer B and Hynynen K 1990 Theoretical and experimental evaluation of a temperature controller for scanned focused ultrasound hyperthermia *Medical Physics* **17** 615-625
- Mahoney K, Fjield T, McDannold N, Clement G, Hynynen K 2001 Comparison of modelled and observed *in vivo* temperature elevations induced by focused ultrasound: implications for treatment planning *Phys. Med. Biol.* **46** 1785-1798
- Malinen M, Huttunen T and Kaipio J P 2002 An optimal control approach for ultrasound induced heating *International Journal of Control* submitted
- Mast T D, Souriau L P, Liu D-L D, Tabei M, Nachman A I, Waag R C 2001 A  $k$ -space method for large-scale models of wave propagation in tissue *IEEE Trans. Ultrason. Ferroelectr. Freq. Control* **48** 341-354
- Mast T D, Hinkelman L M, Metlay, L A, Orr, M J and Waag R C 1999 Simulation of ultrasonic pulse propagation, distortion, and attenuation in the human chest wall *J. Acoust. Soc. Am.* **106**

3665-3677

- Mattingly M, Roemer R B and Devasia S 2000 Exact temperature tracking for hyperthermia: a model-based approach *IEEE Trans. Control Syst. Technol.* **8** 979-992
- McDannold N J, Hynynen K, Wolf D, Wolf G and Jolesz F A 1998 MRI evaluation of thermal ablation of tumors with focused ultrasound *J. Magn. Reson. Imaging* **8** 91-100
- McDannold N J 2002 MRI monitoring of high temperature ultrasound therapy Ph.D. Dissertation, Tufts University, Medford, Massachusetts
- Pennes H H 1948 Analysis of tissue and arterial blood temperatures in the resting human forearm *J. Appl. Phys.* **1** 93-122
- Pierce A D 1994 *Acoustics: an introduction to its physical principles and applications* (Acoustical Society of America)
- Sapareto S A and Dewey W C 1984 Thermal dose determination in cancer therapy *Int. J. Radiation Oncology Biol. Phys.* **10** 787-800
- Stengel R F 1994 *Optimal Control and Estimation* (New York: Dover Publications, inc.)
- VanBaren P and Ebbini E S 1995 Multi-point temperature control during hyperthermia treatments: theory and simulation *IEEE Trans. Biomed. Eng.* **42** 818-827
- Wan H, VanBaren P, Ebbini E S and Cain C A 1996 Ultrasound surgery: comparison of strategies using phased array systems *IEEE Trans. Ultrason. Ferroelectr. Freq. Control* **43** 1085-1098
- Wojcik G, Fornberg B, Waag R, Carcione L, Mould J, Nikodym L and Driscoll T 1997 Pseudospectral methods for large-scale bioacoustic models *IEEE Ultrasonic Symposium Proceeding* 1501-1506